aerospace

MDPI

Article

Experimental Study of Aerodynamic and Bird Exclusion Characteristics of a Branched Turboprop Inlet Under Ground Suction Conditions

Ge Zhou, Zhenlong Wu * and Huijun Tan

College of Energy and Power Engineering, Nanjing University of Aeronautics and Astronautics, Nanjing 210016, China; zhouge19991128@nuaa.edu.cn (G.Z.); tanhuijun@nuaa.edu.cn (H.T.)
* Correspondence: zhenlongwu@nuaa.edu.cn

Abstract

A turboprop aircraft is exposed to the risk of bird strikes during flight, which may have a serious impact on flight safety once the bird is sucked into the engine. In this study, the aerodynamic and bird exclusion characteristics of a branched turboprop inlet were tested on a branched turboprop inlet–bird striking experiment system under ground suction conditions. The ingestion processes of the bird were captured by a high-speed camera system. The static pressure at the inner wall of the inlet during the ingestion process was measured. The results indicate that when a low-speed bird at a large incident angle impacts on the wall of the inlet near the lower lip under ground suction conditions, the bird is easily sucked into the core duct. Conversely, it is more likely to be excluded by the bypass duct. Moreover, when the bird moves into the inlet, the static pressure on the wall of the area where it passes through increases significantly.

Keywords: branched turboprop inlet; bypass duct; aerodynamic characteristic; foreign object exclusion; bird

check for updates

Academic Editor: Roberto Navarro

Received: 27 May 2025
Revised: 2 July 2025
Accepted: 18 July 2025
Published: 19 July 2025

Citation: Zhou, G.; Wu, Z.; Tan, H. Experimental Study of Aerodynamic and Bird Exclusion Characteristics of a Branched Turboprop Inlet Under Ground Suction Conditions. *Aerospace* **2025**, *12*, 640. https://doi.org/10.3390/aerospace12070640

Copyright: © 2025 by the authors. Licensee MDPI, Basel, Switzerland. This article is an open access article distributed under the terms and conditions of the Creative Commons Attribution (CC BY) license (https://creativecommons.org/licenses/by/4.0/).

1. Introduction

In recent years, the growth in demand for civil aviation transportation has led to the rapid development of transport aircraft, especially turboprop aircraft. A turboprop aircraft has the advantages of higher fuel efficiency and greater takeoff thrust [1–3] so that it is widely utilized in short-haul commuter, military transport, and patrol aircraft [4,5]. However, turboprop aircraft may encounter harsh environments during flight in which a variety of foreign objects (bird [6,7], hailstone [8], ice slab [8,9], raindrop [10], and sand [11]) can be sucked into the engine. Foreign objects may cause serious damage to the engine. For example, sand can erode the blades of the propeller and internal structure of the engine, causing a significant reduction in their performance [12,13].

Among these various foreign objects, the size of a bird is the largest, so that it produces more serious damage to the engine. Once this occurs, it often results in a catastrophic accident. First of all, the mixing of the airflow from the inlet and the bird will lead to a decrease in the quality of the flow field, so that the aerodynamic performance parameters of the inlet may be significantly reduced [6,14]. Furthermore, the birds may damage the surface of the propeller and the inlet, so that significant degradation of the structural safety of the aircraft and the aerodynamic performance of the propellers may occur. In addition, if birds are not excluded from the engine, they will cause more serious damage to the internal

structure of the engine [7,15,16]. Therefore, to prevent foreign objects from entering the engine, a kind of branched turboprop inlet is being developed, which is composed of a core duct and a bypass duct [6,17]. The core duct is located at the upper part of the inlet to connect to the compressor; the bypass duct is located at the lower part of the inlet to connect to the atmosphere. Foreign objects can be effectively excluded by the bypass duct through its own inertial force, leaving clean airflow to be conveyed to the core duct.

At present, there has been significant progress in the studies of the aerodynamic characteristics of the branched turboprop engine inlet [6,17–21], and numerical investigation of foreign object exclusion (FOE) within the inlet has developed significantly. However, the experimental investigation of FOE within the inlet remains in its early stages. The research on foreign objects mainly focuses on the deformation of the aircraft structure during the impact of foreign objects on the aircraft [22–26]. As for the study of the trajectory of the foreign object, Michael Papadakis et al. developed a four-degree-of-freedom (4-DOF) computational method to analyze the shedding process of ice slabs with different shapes [27]. Later, they further developed a six-degree-of-freedom (6-DOF) trajectory calculation method to simulate the shedding process of ice slabs from the wing and fuselage of a jet aircraft [28], and conducted a wind tunnel test to measure the trajectory of the ice slab shedding in the airflow [29]. In addition, numerical research on the motion characteristics of foreign objects within the inlet has advanced significantly. Mi et al. have conducted a number of studies on the exclusion characteristics for the branched turboprop engine inlet [9,30,31]. At first, they evaluated the performance of a certain type of turboprop engine inlet with a bypass duct in 2019. A CFD combined with a six-degree-of-freedom simulation method is proposed to comprehensively analyze the impact, exclusion, and interference generated by rigid foreign objects in the inlet [30]. However, this simulation model is based on a fully elastic collision, which is too idealized. In actual flight, the foreign objects will be coupled with the internal flow field after entering the inlet, and the trajectory of the foreign objects will be more complicated. Later, they simulated the process of hailstone and ice slab ingestion into the engine using LSDYNA R10.1.0 in 2020. It was found that ice slabs initially located at the lower lip were susceptible to being sucked into the core duct, thus threatening the engine [31]. What is more, they established a numerical simulation method for the motion of two kinds of fragile foreign objects (ice slab and hailstone) in the turboprop inlet with a bypass duct by combining the unsteady CFD technique, 6-DOF, and CSD impact theory. The exclusion characteristics of the ice-type foreign objects and their impacts on the aerodynamic performances of the inlet were evaluated in detail [9]. Zheng et al. also conducted a lot of studies on the bird exclusion characteristics in a branched turboprop engine inlet [6,14]; they introduced a numerical simulation method coupling the self-developed collision–rebound model, overset mesh, and 6-DOF to calculate the bird exclusion characteristics of a turboprop inlet under propeller interference at a large angle of attack. And through the parametric design method, the exclusion performance of the inlet was optimized [6].

In summary, there are many numerical studies on the aerodynamic characteristics and FOE of the branched turboprop inlet at the moment, whereas experimental studies of FOE in the inlet have rarely been reported. As a result, in this paper, an experimental study of the aerodynamic and bird exclusion characteristics of a branched turboprop inlet with a bypass duct under ground suction conditions based on a branched turboprop inlet–bird striking experiment system is conducted. The bird exclusion characteristics of the inlet and the aerodynamic effects of bird striking on the inlet are discussed. Section 2 presents a detailed description of the experimental setup of the branched turboprop inlet–bird striking experiment. Section 3 describes the terminological definitions in this paper.

Section 4 presents a discussion of the experimental results. Section 5 draws a conclusion of the present study.

2. Experimental Setup

2.1. Test Model

The test model of a branched turboprop engine inlet is composed of a core duct and a bypass duct. The power extraction shaft passes through the core duct, forming a circular cross-section of the core duct. The total pressure rake for the core duct is installed at the aerodynamic interface plane (AIP, located at the outlet of the inlet and the entrance of the compressor) between the inlet and the engine, and the total pressure rake for the bypass duct is at the outlet of the bypass duct. Additionally, static pressure measurement points are arranged on the outer surface of the model to collect the static pressure of the wall. Since one side is used for capturing the motion trajectory of the bird dummy, 26 static pressure measurement points are distributed along the other side, with 6 points on Line1 and 20 points on Line2. Line1 is located on the upper wall of the inlet entrance, and Line2 is positioned on the side of the bypass duct. The test model is shown in Figure 1, and the geometric parameters of the inlet are tabulated in Table 1.

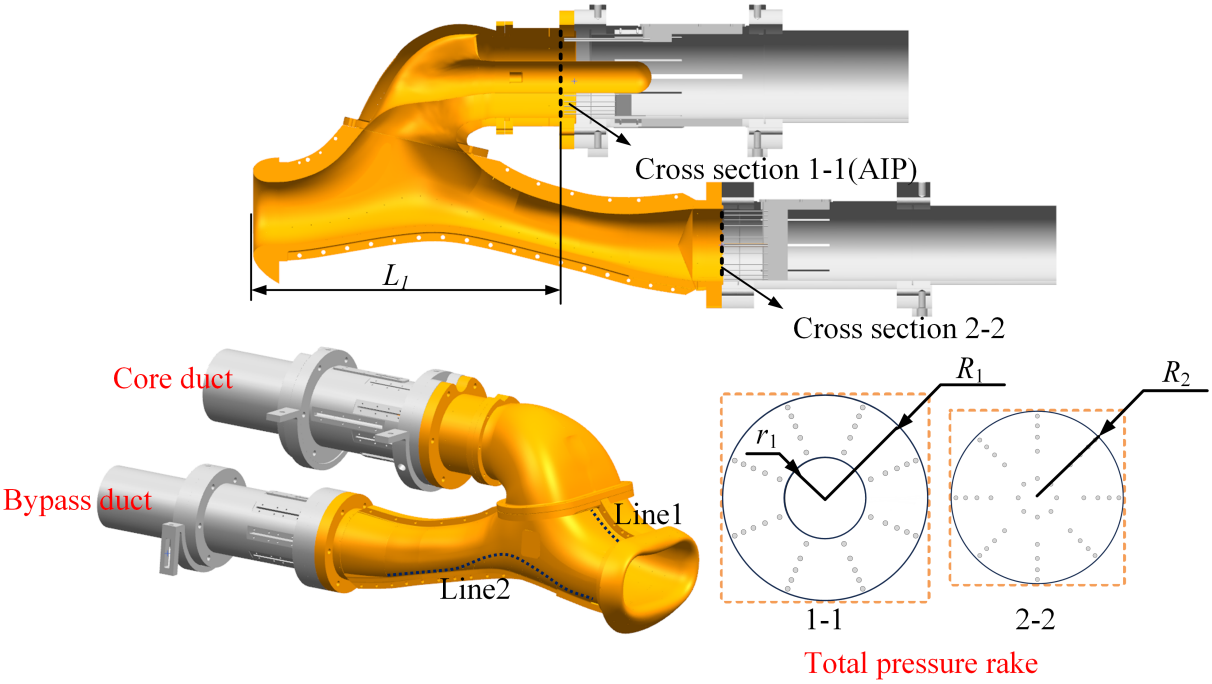


Figure 1. Test model.

Table 1. Geometry parameters of the test model.

Parameter	Units	Value
Core duct outside radius, R_1	mm	48.3
Core duct inside radius, r_1	mm	19
Bypass duct radius, R_2	mm	43
Distance of entrance from AIP, L_1	mm	352.8
Inlet throat area, A_0	mm^2	13,000
Core duct exit area, A_1	mm^2	6195
Bypass duct exit area, A_2	mm^2	5809

2.2. Experimental System

A branched turboprop inlet–bird striking experiment system (Figure 2) is designed to conduct the aerodynamic and exclusion experiment of the branched turboprop inlet under ground suction conditions. The experimental system includes a low-pressure storage tank suction experiment platform, a transparent turboprop inlet model, two total pressure rakes connecting the two ducts, a launcher (Figure 2b), a pressure measurement device (Figure 2c), and a high-speed camera system (Figure 2d).

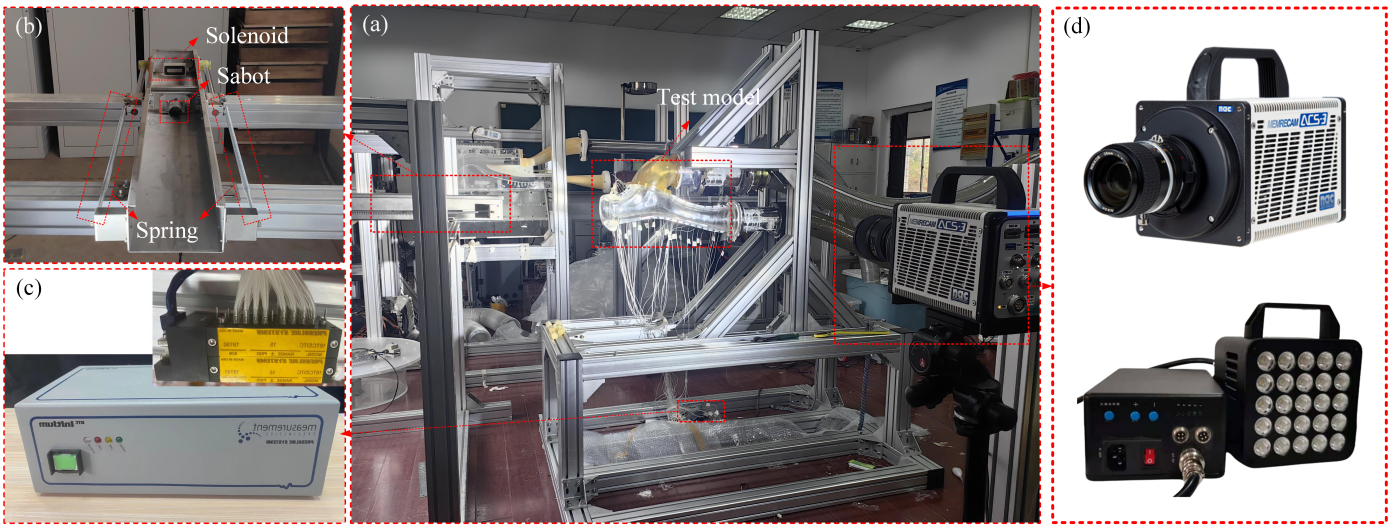


Figure 2. Experimental system: (**a**) branched turboprop inlet–bird striking experiment setup; (**b**) launcher structure; (**c**) pressure measurement device; (**d**) high-speed camera system.

The launcher consists of a projection plate with a sabot, two springs, a solenoid, a slide, and a triggering device. The solenoid is energized so that the projection plate is absorbed by the solenoid. When the experiment is ready, the solenoid is de-energized by controlling the triggering device, and the bird is launched using the elasticity of the spring at an initial velocity of about 1–10 m/s.

The pressure measurement device is an electronically scanned pressure transducer system (ESP-64HD) produced by the PSI company in the United States, with a measurement accuracy of 0.05% of the full scale. Because the measurement range of the ESP modules is 15 psi (103,421 pa), the maximum error of the pressure measurement device is approximately ±52 pa. The high-speed camera system consists of a high-speed camera and an LED light. The high-speed camera is a Memrecam ACS-3 high-speed camera produced by Nac Image Technology Inc. in Japan. It has a maximum of 1 megapixel. At this full frame resolution, the frame rate is up to 30,000 fps, and the maximum speed is up to 220,000 fps, with a maximum frame rate of 250,000 fps at 1280 × 896 resolution and 50,000 fps at 1280 × 448 resolution. The camera is placed on the side of the inlet and equipped with an LED light to enhance the shooting effect. The resolution of the high-speed camera in the experiment is adjusted to 1280 × 896, and the frequency is 10,000 fps.

During the aerodynamic experiment, the air source of the experiment is provided by the low-pressure storage tank suction experiment platform. After reaching the required pressure for the experiment by adjusting the valve, the wall pressure along the inlet and the outlet pressure are collected by the pressure measurement device.

During the exclusion experiment, the wall pressure along the inlet and the outlet pressure without the bird dummy are collected first. Subsequently, the bird dummy is launched by controlling the triggering device. At the same time, the wall pressure along the inlet and the outlet pressure during the motion of the bird are captured. In addition, a high-speed camera system is used to monitor the trajectory of the bird in the inlet. Notably,

a filter is installed at the outlet to prevent birds from entering the suction duct, and the total pressure rakes are removed to protect the probe on the total pressure rakes in this process. The operation conditions required are adjusted by the position of the valve.

2.3. Bird Dummy Selection and Preparation

The bird dummy is modeled as a cylinder made of gelatin with an aspect ratio of 2:1 in this study to keep it consistent with previous studies [22,24,32,33], as shown in Figure 3. The geometry parameters of the bird dummy are shown in Table 2.

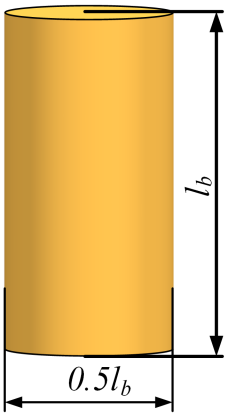


Figure 3. Bird dummy model.

Table 2. Geometry parameters of the bird dummy.

Parameter	Units	Value
Bird dummy length, L_b	m	0.048
Bird dummy weight, M_b	kg	0.021

Based on the formulation of the bird dummy documented in the relevant literature [34], gelatin is utilized to prepare the bird dummy. The elasticity and hardness of the bird dummy are adjusted by modifying the ratios of the water, gelatin powder, and sodium carboxymethylcellulose during the preparation process. Since the bird dummy made from the literature [34] (10:1 ratio of water to gelatin) is too soft, a ratio of 5.5:1 water to gelatin and 4:1 gelatin to sodium carboxymethylcellulose is used to make the bird dummy in this paper. The density of the bird dummy is 950 kg/m^3, and the process of preparation is shown in Figure 4. First, 110 g of water, 20 g of gelatin powder, and 5 g of sodium carboxymethylcellulose are weighed for each preparation. Subsequently, the water is heated to 60 °C, the gelatin powder is stirred until completely dissolved, and then the sodium carboxymethylcellulose is stirred until completely dissolved. Finally, the stirred gelatin liquid is poured into the mold. After 8–10 h of refrigeration, the mold is opened. The right length of the bird dummy is cut and wrapped with a plastic wrap for refrigeration. The prepared bird dummies have a mass range of 20–22 g, a length of 48 $\pm$ 2 mm, and a base diameter of 24 mm.

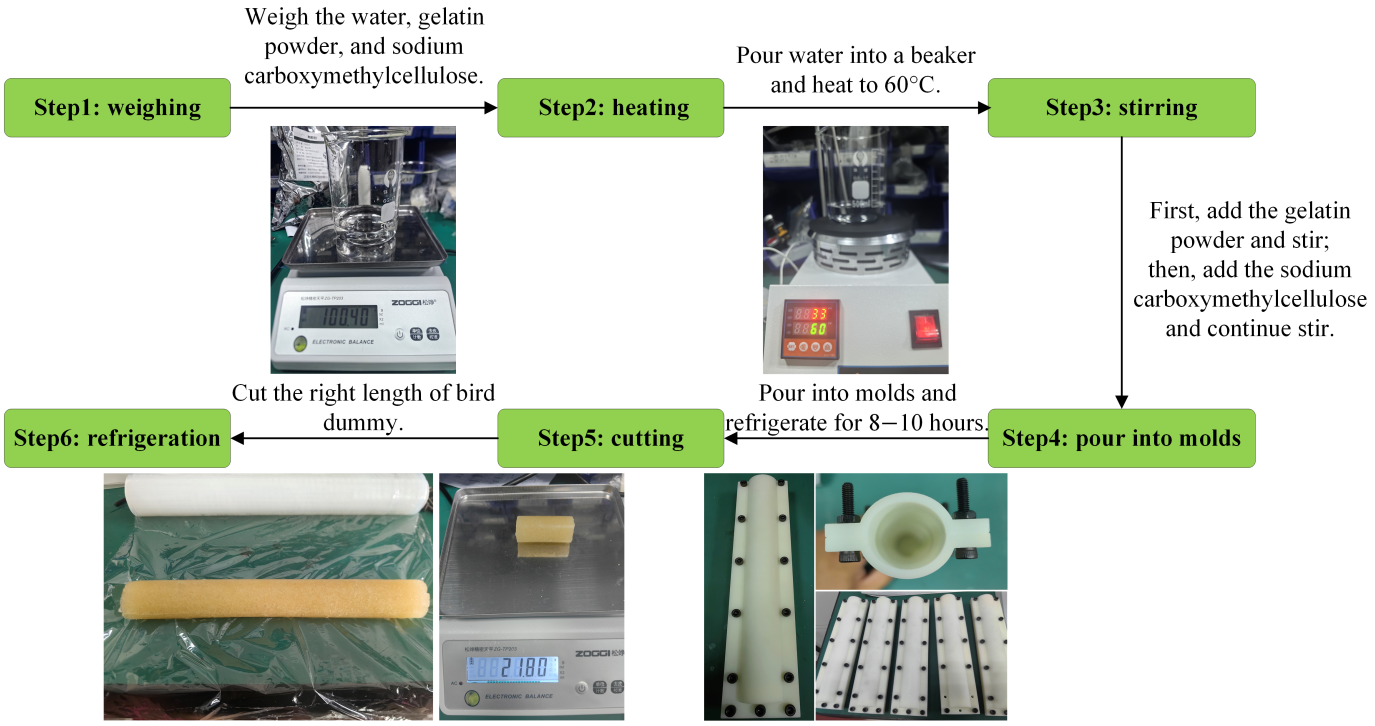


Figure 4. Process of the bird dummy preparation.

3. Terminological Definitions

Some basic concepts and terminologies need to be defined before the discussion of the results.

The total pressure recovery coefficient, σ, is defined as

$$\sigma = p^*_{\mathrm{AIP}}/p^*_0. \tag{1}$$

where p^*_{AIP} is the average total pressure at the AIP, and p^*_0 is the freestream total pressure.

The total pressure distortion index (DC60) is defined as

$$\mathrm{DC60} = \frac{p^*_{\mathrm{min60}} - p^*_{\mathrm{AIP}}}{q_{av}}. \tag{2}$$

where p^*_{min60} is the minimum total pressure in any sector region with the azimuthal angle of 60°, and q_{av} is the average dynamic pressure at the AIP.

The Mach number at the AIP, Ma_{AIP}, is defined as

$$Ma_{\mathrm{AIP}} = \sqrt{\frac{2}{k-1}\left[\left(p^*_{\mathrm{AIP}}/p_{\mathrm{AIP}}\right)^{\frac{k-1}{k}} - 1\right]}. \tag{3}$$

where p_{AIP} is the static pressure at the AIP, respectively. The ratio of specific heat of air k is 1.4.

The Mach number at the outlet of the bypass duct, $Ma_{\text{B-duct}}$, is defined as

$$Ma_{\text{B-duct}} = \sqrt{\frac{2}{k-1}\left[\left(p^*_{\text{B-duct}}/p_{\text{B-duct}}\right)^{\frac{k-1}{k}} - 1\right]}. \tag{4}$$

where $p^*_{\text{B-duct}}$ and $p_{\text{B-duct}}$ are the average total pressure and static pressure at the outlet of the bypass duct, respectively.

4. Results and Discussion

In this study, the aerodynamic and bird exclusion characteristics of the branched turboprop inlet under ground suction conditions are comprehensively studied by adjusting the outlet pressure of the core duct and the bypass duct. The following subsections extend a detailed discussion of the aerodynamic and bird exclusion characteristics by changing the Ma_{AIP} and $Ma_{B\text{-}duct}$.

4.1. Aerodynamic Characteristics of the Inlet

By controlling the valves to adjust the suction pressure downstream of the core duct and bypass duct, the performance of the inlet under different Ma_{AIP} and different $Ma_{B\text{-}duct}$ is obtained. Table 3 and Figure 5 show the total pressure recovery coefficient σ and total pressure distortion |DC60| of the AIP for different operating conditions, where the velocity of the freestream is 0 m/s. First, it can be found that σ and |DC60| decrease as Ma_{AIP} increases under ground suction conditions. The reason for the decrease in σ is that the static pressure level in the core duct decreases with the increase in engine operating parameters, which leads to an overall decrease in the quality of the outlet flow field, whereas the reason for the decrease in |DC60| is that the airflow in the inlet is mixed more quickly with the increase in engine operating parameters, which leads to a decrease in the uniformity of the airflow. Second, $Ma_{B\text{-}duct}$ has a significant effect on the aerodynamic performance of the branched turboprop inlet. As $Ma_{B\text{-}duct}$ increases, σ decreases, |DC60| increases, and the inlet aerodynamic performance decreases significantly. In addition, the friction loss in the inlet increases with Ma_{AIP} and $Ma_{B\text{-}duct}$ increasing, which also contributes to the decrease in σ of the inlet.

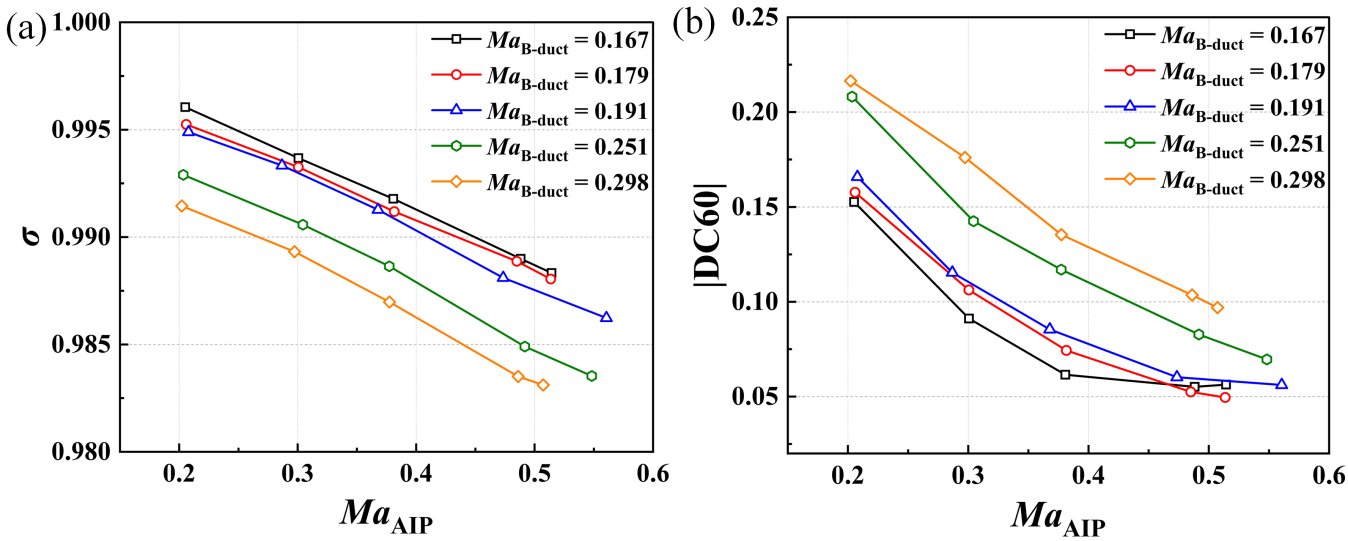


Figure 5. Aerodynamic performance of the inlet at different Ma_{AIP} and $Ma_{B\text{-}duct}$: (**a**) σ; (**b**) |DC60|.

Figure 6 shows the distribution of the static pressure along the inlet when $Ma_{B\text{-}duct}$ = 0.191 and Ma_{AIP} is different, whereas the distribution of the static pressure along the inlet when $Ma_{AIP} \approx 0.5$ and $Ma_{B\text{-}duct}$ is different is shown in Figure 7. First, it can be seen from Figure 6 that as $Ma_{B\text{-}duct}$ increases, the static pressure along Line1 and Line2 generally decreases. Similarly, it is also seen from Figure 7 that as $Ma_{B\text{-}duct}$ increases, the static pressure along Line1 and Line2 decreases. In addition, it can be found from Figure 7 that the static pressure along Line1 when $Ma_{B\text{-}duct}$ = 0.257 is smaller than that when $Ma_{B\text{-}duct}$ = 0.298, which is due to the small difference of Ma_{AIP}. It also indicates that there is a coupling effect between the core duct and the bypass duct.

Table 3. AIP performance of the test results.

Run	Ma_{AIP}	$Ma_{B\text{-}duct}$	σ	|DC60|
1	0.514	0.167	0.9883	0.0563
2	0.488	0.167	0.9890	0.0551
3	0.381	0.167	0.9918	0.0615
4	0.301	0.167	0.9937	0.0911
5	0.205	0.167	0.9960	0.1526
6	0.514	0.179	0.9880	0.0496
7	0.485	0.179	0.9889	0.0524
8	0.382	0.179	0.9912	0.0744
9	0.300	0.179	0.9933	0.1062
10	0.206	0.179	0.9952	0.1577
11	0.561	0.191	0.9862	0.0561
12	0.474	0.191	0.9881	0.0602
13	0.368	0.191	0.9913	0.0854
14	0.287	0.191	0.9933	0.1154
15	0.208	0.191	0.9949	0.1658
16	0.548	0.257	0.9835	0.0696
17	0.492	0.257	0.9849	0.0827
18	0.377	0.257	0.9886	0.1170
19	0.304	0.257	0.9906	0.1425
20	0.203	0.257	0.9929	0.2081
21	0.507	0.298	0.9831	0.0969
22	0.486	0.298	0.9835	0.1036
23	0.377	0.298	0.9870	0.1354
24	0.297	0.298	0.9893	0.1761
25	0.202	0.298	0.9914	0.2165
26	0.441	0.331	0.9832	0.1316
27	0.381	0.331	0.9853	0.1498
28	0.285	0.331	0.9886	0.1939
29	0.510	0.122	0.9897	0.0659
30	0.533	0.182	0.9871	0.0559

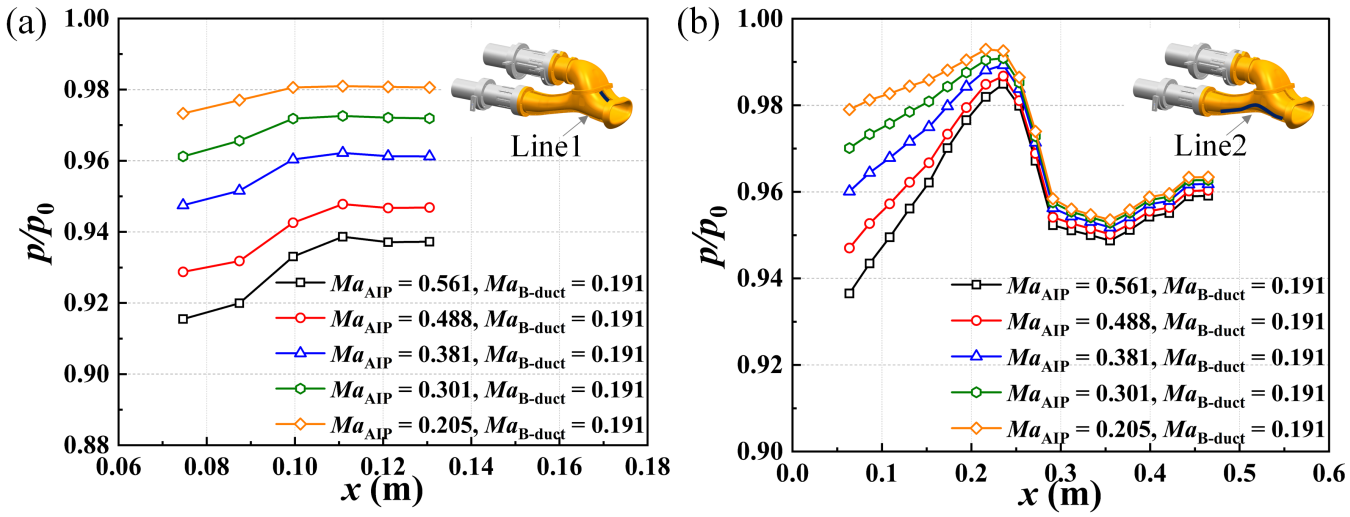


Figure 6. Static pressure along the inlet at different Ma_{AIP}: (**a**) Line1; (**b**) Line2.

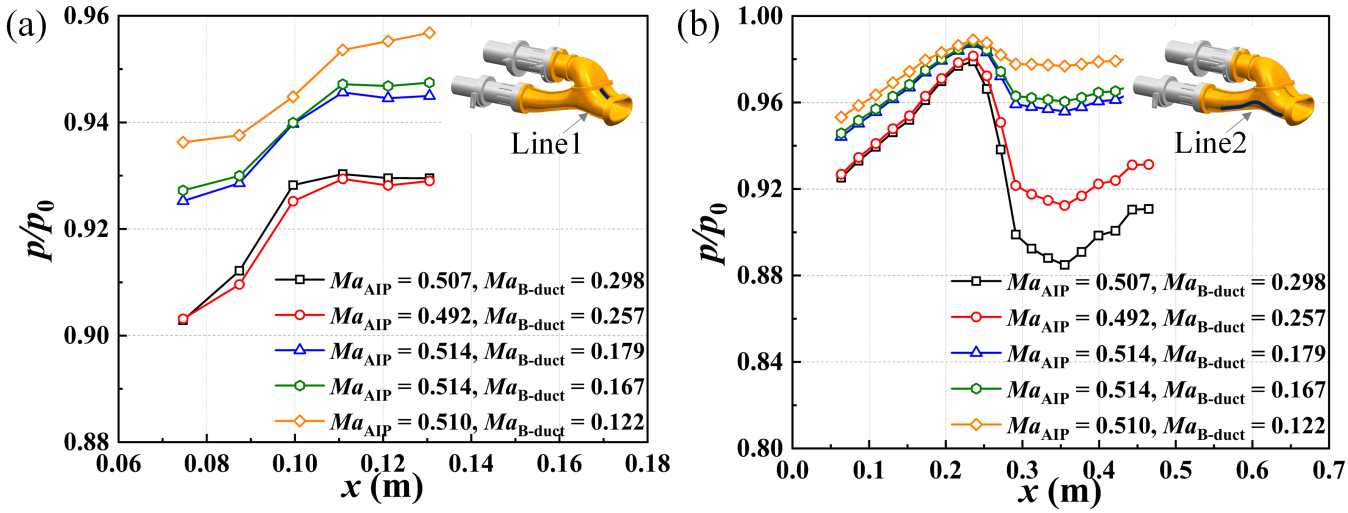


Figure 7. Static pressure along the inlet at different $Ma_{\text{B-duct}}$: (**a**) Line1; (**b**) Line2.

4.2. Exclusion Characteristics of the Inlet

By changing the suction pressure downstream of the core duct and bypass duct, the motion of bird dummies in the inlet under different Ma_{AIP} and different $Ma_{\text{B-duct}}$ is obtained. Table 4 shows the motion and exclusion of the bird dummy in the inlet under ground suction conditions with different engine operating parameters. In Table 4, the repeatability tests were conducted for several operating conditions. The nominal Ma_{AIP} and the nominal $Ma_{\text{B-duct}}$ for Cases 4, 5, and 6 are 0.35 and 0.2, respectively. The nominal Ma_{AIP} and the nominal $Ma_{\text{B-duct}}$ for Cases 7 and 8 are 0.3 and 0.2, respectively. The nominal Ma_{AIP} and the nominal $Ma_{\text{B-duct}}$ for Cases 9, 10, and 11 are 0.25 and 0.2, respectively. It can be found that the exclusions are all the same when the incident angle of the bird is similar. When the incident angle of the bird is more than 13°, it is easy for it to enter the core duct.

Table 4. The motion and exclusion characteristics of bird dummies in the inlet under ground suction conditions with different engine operating parameters.

Case	V_{bird} (m/s)	α_{bird}	Ma_{AIP}	$Ma_{\text{B-duct}}$	Outcome	Excluded?
1	3.81	−9.87°	0.494	0.208	A	Yes
2	6.54	−1.43°	0.461	0.209	B	Yes
3	5.27	1.26°	0.414	0.208	D	No
4	3.82	−3.28°	0.355	0.215	A	Yes
5	8.48	−2.95°	0.334	0.211	A	Yes
6	5.34	−1.17°	0.333	0.200	C	Yes
7	4.74	0°	0.320	0.210	A	Yes
8	6.37	−3.83°	0.283	0.205	A	Yes
9	6.73	−3.01°	0.247	0.208	A	Yes
10	1.67	0°	0.221	0.202	C	Yes
11	4.77	−13.83°	0.221	0.210	D	No
12	5.77	−1.08°	0.352	0.173	A	Yes
13	5.44	−9.94°	0.353	0.263	A	Yes
14	4.32	−16.84°	0.450	0.176	D	No
15	3.81	−10.01°	0.462	0.235	A	Yes
16	3.76	−2.49°	0.452	0.259	A	Yes

Note that in the outcome column, A represents "the bird dummy first impacted the bulge of the bypass duct, then impacted the lower surface of the diverter and entered the bypass duct", B "the bird dummy first impacted the upper lip, then impacted the bulge of the bypass duct, and lastly impacted the lower surface of the diverter and entered the bypass duct", C "the bird dummy impacted the lower surface of the diverter and entered the bypass duct", D "the bird dummy entered the core duct".

Furthermore, it is seen from Table 4 that there are three cases in which the bird dummy enters the core duct in all the tests. Moreover, there are four categories (A, B, C, and D) of impacting outcomes for the bird. A, B, and C are the situations in which the bird enters the bypass duct, and D is the situation in which the bird enters the core duct. The first category is that the bird impacted the bulge of the bypass duct, then impacted the lower surface of the diverter, and entered the bypass duct (A) in Cases 1, 4, 5, 7, 8, 9, 12, 13, 15, and 16, as indicated in Figure 8a. It is worth noting that Figure 8 shows the position of the bird dummy at intervals of 7.5 ms. The second category is that the bird impacted the upper lip, then impacted the bulge of the bypass duct, then impacted the lower surface of the diverter, and entered the bypass duct (B) in Case 2, as indicated in Figure 8b. The third category is that the bird impacted the lower surface of the diverter, and then entered the bypass duct (C) in Cases 6 and 10, as indicated in Figure 8c. The motion patterns entering the bypass duct of the three categories are summarized in Figure 9.

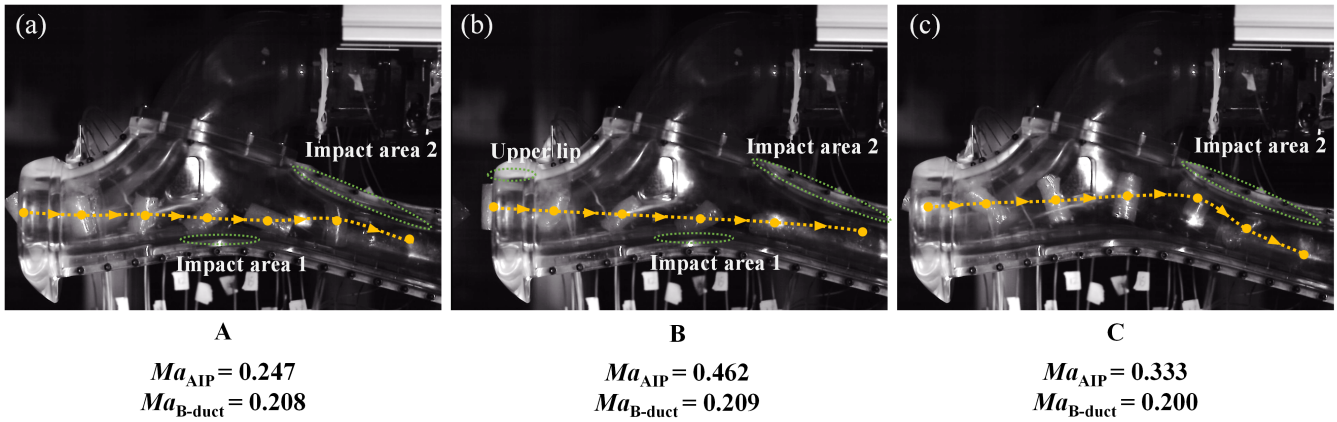


Figure 8. Three categories of impacting outcomes for the bird dummy entering the bypass duct: (**a**) A; (**b**) B; (**c**) C.

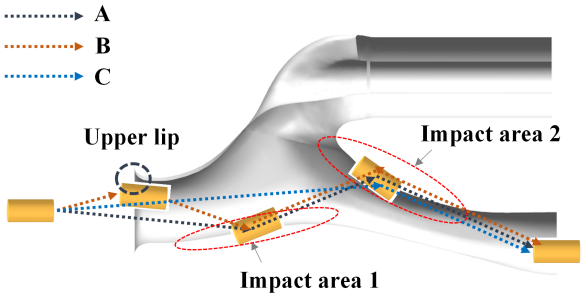
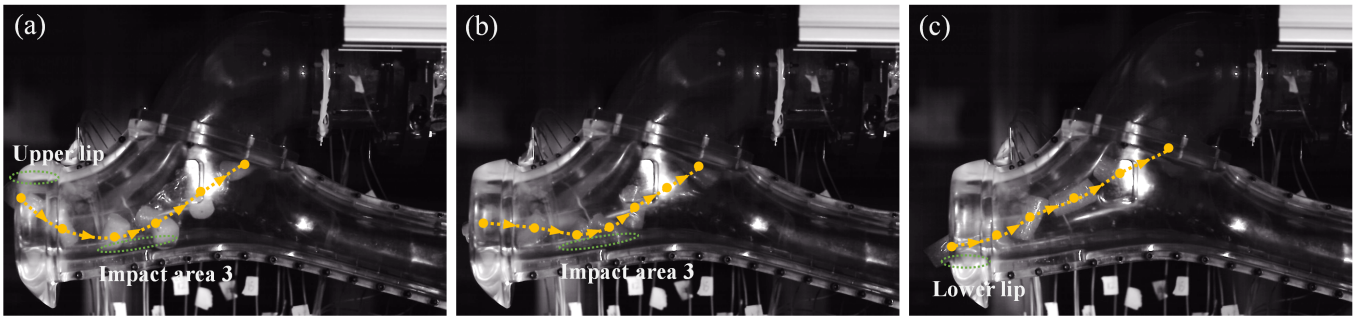


Figure 9. Illustration of the motion of the bird entering the bypass duct in the inlet.

The fourth category is that the bird entered the core duct (D) in Cases 3, 11, and 14, which consists of three specific situations: (1) the bird entered the core duct without any contact with the wall in Case 3, as indicated in Figure 10a; (2) the bird impacted the upper lip, then impacted the lower wall of the inlet, and entered the core duct in Case 11, as indicated in Figure 10b; and (3) the bird impacted the lower lip, then entered the core duct in Case 14, as indicated in Figure 10c. Notably, Figure 10 shows the position of the bird dummy at intervals of 7.5 ms. The motion patterns entering the core duct of the three situations are summarized in Figure 11.



D-1
$Ma_{AIP} = 0.414$
$Ma_{B\text{-}duct} = 0.208$

D-2
$Ma_{AIP} = 0.221$
$Ma_{B\text{-}duct} = 0.210$

D-3
$Ma_{AIP} = 0.450$
$Ma_{B\text{-}duct} = 0.176$

Figure 10. Three categories of impacting outcomes for the bird dummy entering the core duct: (**a**) D-1; (**b**) D-2; (**c**) D-3.

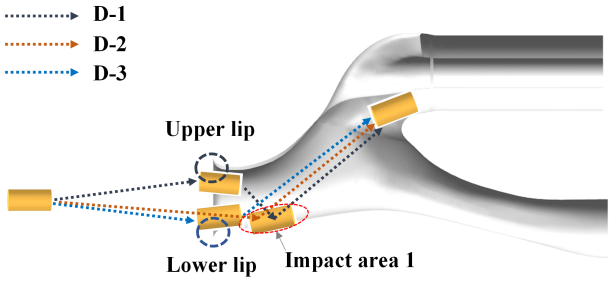


Figure 11. Illustration of the motion of the bird entering the core duct in the inlet.

In addition, it can be found by comparing Figures 8 and 10 that under the three situations of entering the bypass duct, the position where the bird impacts the wall of the inlet is relatively far away from the lower lip. However, under the three situations of entering the core duct, the bird always impacted the wall of the inlet near the lower lip, either in the first collision or the second collision. Therefore, for the birds that dive downward, the profile of the lower surface of the inlet has a greater impact on the exclusion performance of the inlet. In the future, the lower surface of the inlet can be optimized and designed by using the parametric design method in the literature [6].

4.3. Aerodynamic Effects of the Bird on the Inlet

Table 5 provides the time-averaged results of the static pressure at the outlet with and without the bird dummy under ground suction conditions, whereas Figures 12 and 13 compare the static pressure at the outlet with and without the bird dummy at different Ma_{AIP} and $Ma_{B\text{-}duct}$, respectively. It can be found that when the bird dummy enters the bypass duct, the static pressure of its outlet increases significantly, and the static pressure at the outlet of the core duct also increases slightly. The reason for this is that there is a blocking effect of the bird dummy on the airflow, and the flow rate in the bypass duct decreases significantly. Similarly, when the bird dummy enters the core duct, the static pressure at the outlet of the core duct increases significantly, and the static pressure at the outlet of the bypass duct increases slightly.

Figures 14 and 15 compare the static pressure along the inlet with and without the bird dummy ($Ma_{B\text{-}duct} \approx 0.21$) in the inlet with different Ma_{AIP}, and the static pressure along the inlet with and without the gelatin bird ($Ma_{AIP} \approx 0.45$) in the inlet with different $Ma_{B\text{-}duct}$, respectively. The static pressure along the inlet with the presence of the bird dummy is a time-averaged result from the time of entry of the bird dummy into the inlet up to the exclusion process.

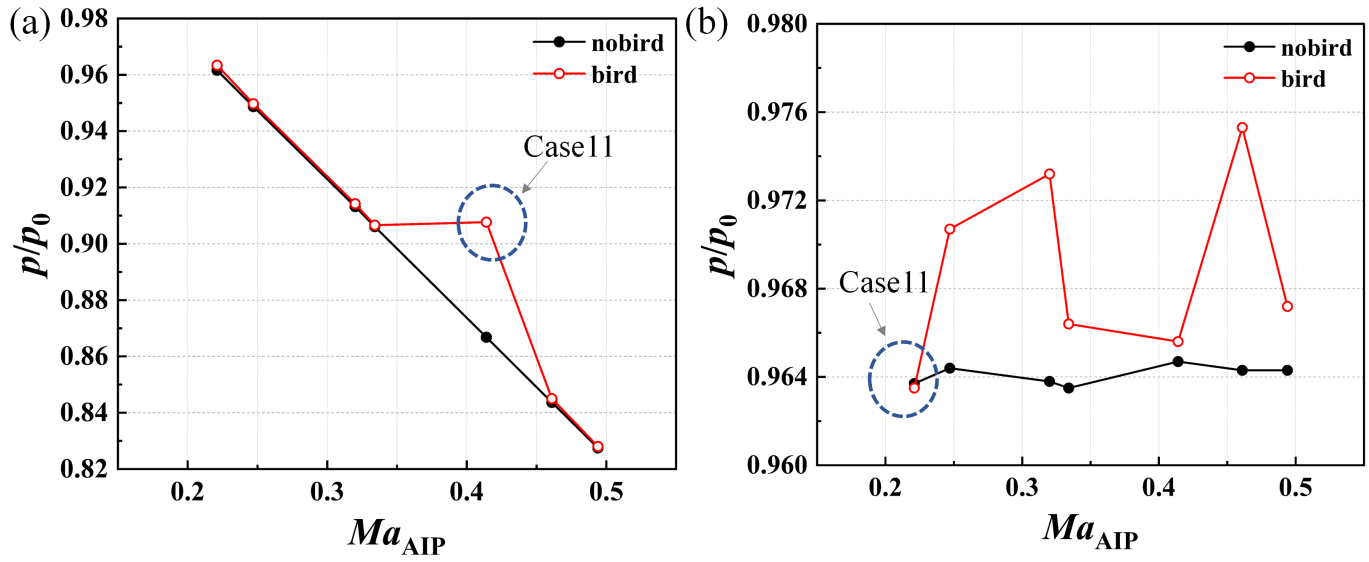


Figure 12. Comparison of static pressure at the outlet with and without the bird dummy at different Ma_{AIP}: (**a**) outlet of the core duct; (**b**) outlet of the bypass duct.

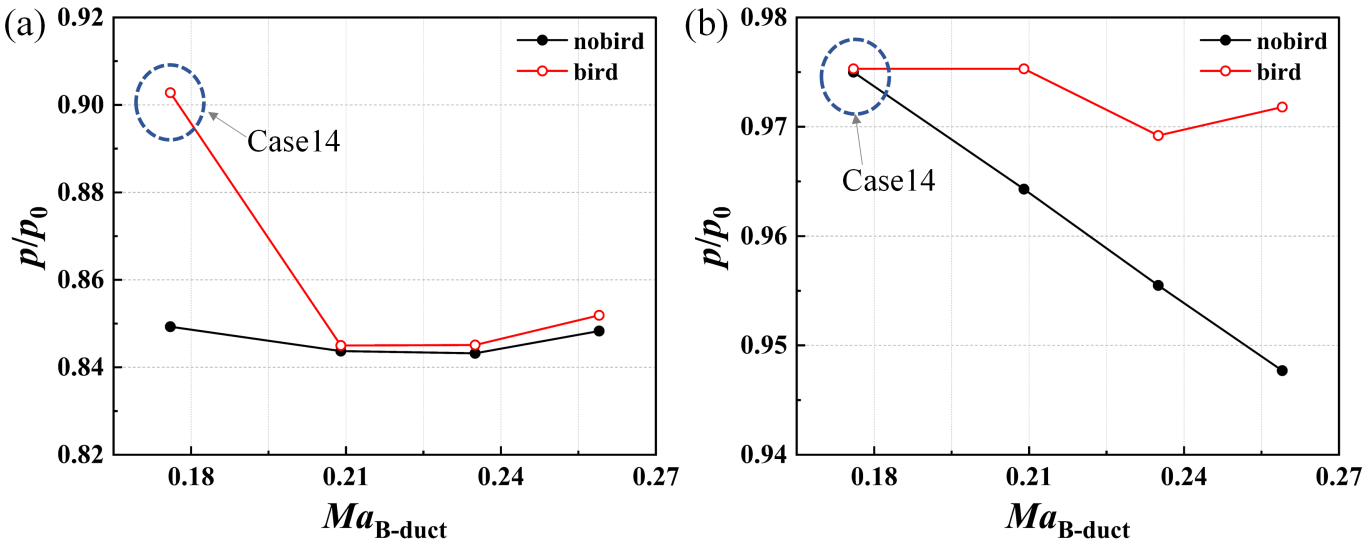


Figure 13. Comparison of static pressure at the outlet with and without the bird dummy at different $Ma_{B\text{-}duct}$: (**a**) outlet of the core duct; (**b**) outlet of the bypass duct.

It can be observed from Figures 14 and 15 that the static pressures on Line1 and Line2 increase during the motion of the bird dummy in the inlet, regardless of which duct the bird dummy enters. The reason for this is that when the bird enters the inlet, it blocks the flow in the inlet, which leads to a reduction in the flow velocity in the inlet. Furthermore, for the case where the bird enters the bypass duct, when the bird enters the inlet, the increase in pressure on Line1 is small, the increase in pressure on the first half of Line2 ($x < 0.25$) is small, and the increase in pressure on the second half of Line2 ($x > 0.25$) is large, which can indicate that the bird enters the bypass duct through the perspective of the aerodynamics as well. For the case of the bird entering the core duct, after the bird enters the inlet, the increase in pressure on Line1 is larger, the increase in pressure in the first half of Line2 ($x < 0.2$) is larger, and the increase in pressure in the second half of Line2 ($x > 0.2$) is smaller. Therefore, it can be concluded that when the bird moves into the inlet, the static pressure on the wall of the area where it passes through increases.

Table 5. Comparison of static pressure at the outlet under ground suction conditions with and without the bird dummy.

Case	Ma_{AIP}	$Ma_{B\text{-}duct}$	p_{AIP}/p_0	$p_{B\text{-}duct}/p_0$	Is There a Bird?
1	0.494	0.208	0.8275	0.9643	No
			0.8280	0.9672	Yes
2	0.461	0.209	0.8437	0.9643	No
			0.8450	0.9753	Yes
3	0.414	0.208	0.8668	0.9647	No
			0.9077	0.9656	Yes
4	0.355	0.215	0.8959	0.9622	No
			0.8961	0.9644	Yes
5	0.334	0.211	0.9061	0.9635	No
			0.9066	0.9664	Yes
6	0.333	0.200	0.9068	0.9673	No
			0.9067	0.9746	Yes
7	0.320	0.210	0.9132	0.9638	No
			0.9142	0.9732	Yes
8	0.283	0.205	0.9311	0.9654	No
			0.9318	0.9718	Yes
9	0.247	0.208	0.9487	0.9644	No
			0.9497	0.9707	Yes
10	0.221	0.202	0.9619	0.9665	No
			0.9629	0.9770	Yes
11	0.221	0.210	0.9616	0.9637	No
			0.9634	0.9635	Yes
12	0.352	0.173	0.8976	0.9758	No
			0.8986	0.9804	Yes
13	0.353	0.263	0.8968	0.9465	No
			0.8997	0.9742	Yes
14	0.450	0.176	0.8493	0.9750	No
			0.9028	0.9753	Yes
15	0.462	0.235	0.8432	0.9555	No
			0.8451	0.9692	Yes
16	0.452	0.259	0.8483	0.9477	No
			0.8519	0.9718	Yes

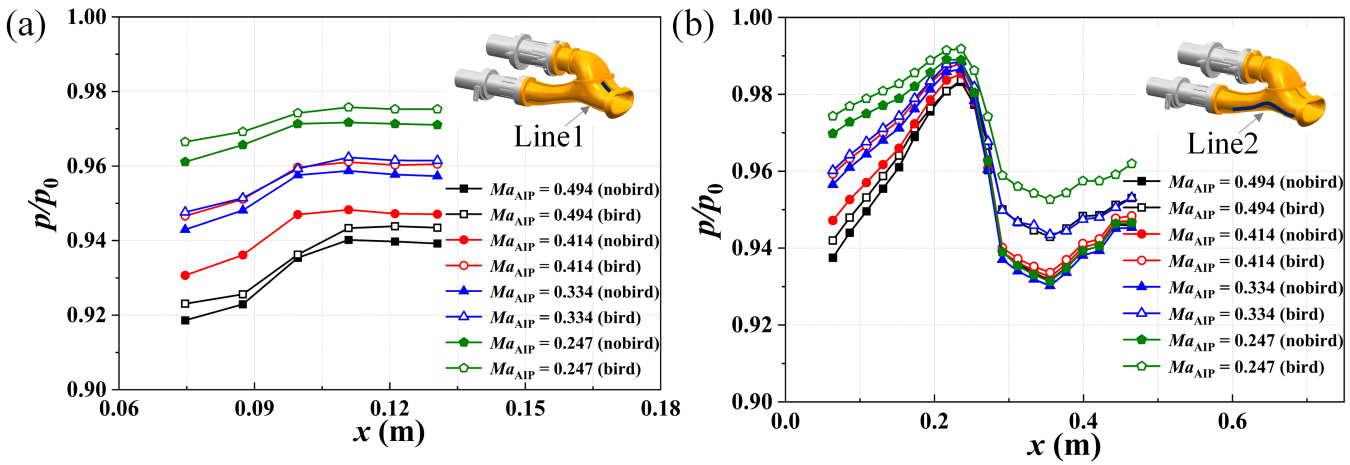


Figure 14. Comparison of static pressure with and without the bird dummy along the inlet at different Ma_{AIP}. (**a**) Line1; (**b**) Line2.

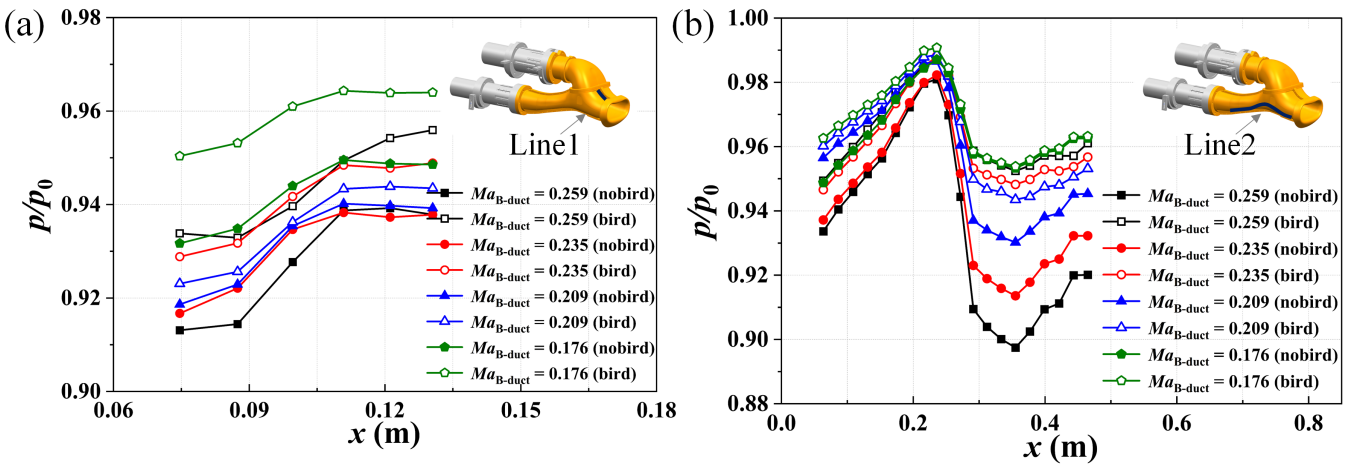


Figure 15. Comparison of static pressure with and without the bird dummy along the inlet at different $Ma_{\text{B-duct}}$. (**a**) Line1; (**b**) Line2.

Overall, birds entering the core duct mainly have a significant effect on the static pressure at the outlet and the static pressure along the core duct, while having little effect on the bypass duct. Conversely, birds entering the bypass duct mainly have a significant effect on the static pressure at the outlet and the static pressure along the bypass duct, while having little effect on the core duct.

5. Conclusions

This paper presents an experimental study of the aerodynamic and bird exclusion characteristics of a branched turboprop inlet on a branched turboprop inlet–bird striking experiment system under ground suction conditions. Its ingestion outcomes were captured and monitored by a high-speed camera system, and the aerodynamic effects of the bird were monitored by a pressure measurement device. The conclusions are as follows:

(1) As Ma_{AIP} increases, σ and |DC60| gradually decrease when $Ma_{\text{B-duct}}$ is certain under ground suction conditions. However, when Ma_{AIP} keeps constant, σ gradually decreases and |DC60| gradually increases as $Ma_{\text{B-duct}}$ increases. Moreover, as both Ma_{AIP} and $Ma_{\text{B-duct}}$ increase, the static pressure along the inlet decreases.

(2) The exclusion of birds is most significantly affected by the incident angle, with all birds excluded at incident angles less than 10°. The motion of the bird dummy entering the bypass duct within the inlet is described in three categories, "impacting the bulge of the bypass duct–impacting the lower surface of the diverter–entering the bypass duct", "impacting the upper lip–impacting the bulge of the bypass duct–impacting the lower surface of the diverter–entering the bypass duct", and "impacting the lower surface of the diverter–entering the bypass duct".

(3) When a low speed bird at a large incident angle impacts on the wall of the inlet near the lower lip under ground suction conditions, the bird is easily sucked into the core duct. Conversely, it is more likely to be excluded by the bypass duct. The motion of the bird entering the core duct within the inlet can also be classified into three categories: "impacting the upper lip–impacting in front of the bulge of the bypass duct–entering the core duct", "impacting in front of the bulge of the bypass duct–entering the core duct", and "impacting the lower lip–entering the core duct".

(4) The static pressure on the wall of the area where it passes through increases significantly as the bird is ingested into the inlet; birds entering the core duct mainly have a significant effect on the static pressure at the outlet and the static pressure along the core duct, while having little effect on the bypass duct. Conversely, birds entering the

bypass duct mainly have a significant effect on the static pressure at the outlet and the static pressure along the bypass duct, while having little effect on the core duct.

Author Contributions: Conceptualization, G.Z. and Z.W.; methodology, G.Z. and Z.W.; software, G.Z.; validation, G.Z.; formal analysis, Z.W.; investigation, G.Z.; resources, H.T.; data curation, G.Z.; writing—original draft preparation, G.Z.; writing—review and editing, Z.W.; visualization, G.Z.; supervision, Z.W.; project administration, H.T.; funding acquisition, H.T. All authors have read and agreed to the published version of the manuscript.

Funding: This study was supported by the Civil Airplane Technology Development Program of China (No. MJ-2020-F-10).

Data Availability Statement: The data presented in this study are available on request from the corresponding author.

Conflicts of Interest: The authors declare that they have no conflicts of interest in this work.

Nomenclature

A_0	Inlet throat area
A_1	Core duct exit area
A_2	Bypass duct exit area
DC60	Total pressure distortion index
k	Ratio of specific heat of air
L_b	Bird dummy length
L_1	Distance of entrance from the AIP
M_b	Bird dummy weight
Ma_{AIP}	Mach number at the AIP
$Ma_{\text{B-duct}}$	Mach number at the outlet of the bypass duct
p_{AIP}	Average static pressure at the AIP
p^*_{AIP}	Average total pressure at the AIP
$p_{\text{B-duct}}$	Average static pressure at the outlet of the bypass duct
$p^*_{\text{B-duct}}$	Average total pressure at the outlet of the bypass duct
p_0	Freestream static pressure
p^*_0	Freestream total pressure
p^*_{min60}	Minimum total pressure in any sector region with the azimuthal angle of 60°
q_{av}	Average dynamic pressure at the AIP
R_1	Core duct outside radius
R_2	Bypass duct radius
r_1	Core duct inside radius
V_{bird}	Incident velocity of the bird
α_{bird}	Incident angle of the bird
σ	Total pressure recovery coefficient
AIP	Aerodynamic interface plane
CFD	Computational fluid dynamics
ESP	Electronically scanned pressure
FOE	Foreign object exclusion
PSI	PRESSURE SYSTEMS INTERNATIONAL INC.
6–DOF	Six–degree–of–freedom

References

1. Balli, O.; Hepbasli, A. Energetic and exergetic analyses of t56 turboprop engine. *Energy Convers. Manag.* **2013**, *73*, 106–120. [CrossRef]
2. Aygun, H. Effects of air to fuel ratio on parameters of combustor used for gas turbine engines: Applications of turbojet, turbofan, turboprop and turboshaft. *Energy* **2024**, *305*, 132346. [CrossRef]

3. Voskuijl, M.; Van Bogaert, J.; Rao, A.G. Analysis and design of hybrid electric regional turboprop aircraft. *CEAS Aeronaut. J.* **2018**, *9*, 15–25. [CrossRef]
4. Saravanamuttoo, H. Modern turboprop engines. *Prog. Aerosp. Sci.* **1987**, *24*, 225–248. [CrossRef]
5. Balli, O. Advanced exergy analyses of an aircraft turboprop engine (tpe). *Energy* **2017**, *124*, 599–612. [CrossRef]
6. Zheng, G.; Tan, H.; Wu, Z.; Zhang, F.; Zhang, Y.; Luo, G. Aerodynamics and bird ingestion characteristics of a bulge-adjustable turboprop engine inlet. *Aerosp. Sci. Technol.* **2024**, *144*, 108777. [CrossRef]
7. Meguid, S.A.; Mao, R.H.; Ng, T.Y. FE analysis of geometry effects of an artificial bird striking an aeroengine fan blade. *Int. J. Impact Eng.* **2008**, *35*, 487–498. [CrossRef]
8. Zhou, G.; Zhou, H.; Wu, Z.; Tan, H.; Qin, W. Ice object exclusion characteristics of turboshaft engine inlet under helicopter/inlet integration conditions. *Aerospace* **2024**, *12*, 458. [CrossRef]
9. Mi, B. A CFD–CSD coupling method for simulating the dynamic impact and expulsion of fragile foreign objects from the 'inlet–bypass duct'junction of a turboprop aircraft. *Eng. Appl. Comput. Fluid Mech.* **2022**, *16*, 73–94.
10. Wu, Z.; Shi, Z.; Sun, S.; Tan, H. Two-phase flow characteristics inside a serpentine inlet in heavy rain. *Phys. Fluids* **2025**, *37*. [CrossRef]
11. Li, C.; Bin, G.; Li, J.; Yang, P.; Wang, W. Influence of inlet distortion on the wear of aero-compressor blades. *Int. J. Mech. Sci.* **2022**, *120*, 107551. [CrossRef]
12. Mohamed, B.; Ahmed, F.; Galal, B. Effect of erodent particle initial velocity on the erosion of propeller blades for turboprop engines. In Proceedings of the 27th Joint Propulsion Conference, Sacramento, CA, USA, 24–26 June 1991.
13. Mohamed, B.; Ahmed, F.; Galal, B. Numerical simulation of the aerodynamic behavior of propeller blades at subsonic conditions. In Proceedings of the 27th Joint Propulsion Conference, Sacramento, CA, USA, 24–26 June 1991.
14. Zhou, H.; Wu, Z.; Tan, H.; Zheng, G.; Zhang, F.; Luo, G.; Chen, W. Numerical simulation on bird ingestion characteristics from engine inlet of turboprop aircraft. *J. Aerosp. Power* **2024**, *39*, 202300831.
15. Zhang, D.; Fei, Q. Effect of bird geometry and impact orientation in bird striking on a rotary jet-engine fan analysis using SPH method. *Aerosp. Sci. Technol.* **2016**, *54*, 320–329. [CrossRef]
16. Mao, R.H.; Meguid, S.A.; Ng, T.Y. Finite element modeling of a bird striking an engine fan blade. *J. Aircr.* **2007**, *44*, 583–596. [CrossRef]
17. Zheng, G.; Wu, Z.; Tan, H.; Zhang, Y.; Wang, K. Design and examination of a turboprop inlet with scavenge duct. *Chin. J. Aeronaut.* **2023**, *36*, 32–42. [CrossRef]
18. Barta, A.; Bennett, W.; Vittal, B.; Krishnan, M. Design and development of a compact bifurcated turboprop inlet. In Proceedings of the 27th Joint Propulsion Conference, Sacramento, CA, USA, 24–26 June 1991.
19. Ruiz-Calavera, L.; Funes-Sebastian, D.; Perdones-Diaz, D. Powered model wind tunnel tests of a high-offset subsonic turboprop air intake. In Proceedings of the 46th AIAA/ASME/SAE/ASEE Joint Propulsion Conference & Exhibite, Nashville, TN, USA, 25–28 July 2010.
20. Gula, P.; Ulma, D.; Zurek, K.; Zurawski, R. Challenges of turboprop engine installation on small aircraft. *Aircr. Eng. Aerosp. Technol.* **2019**, *91*, 938–948. [CrossRef]
21. Zheng, G.; Wu, Z.; Tan, H.; Ren, J.; Zhang, Y.; Zhou, G. Aerodynamic study of a bifurcated turboprop engine inlet with a propeller for flow at ground suction conditions. *Aerosp. Sci. Technol.* **2024**, *155*, 109720. [CrossRef]
22. Luo, G.; Xu, Z.; Shen, H.; Chen, W.; Zhang, H. Experimental study on the impact load of internally supported gelatin bird projectiles. *Eng. Fail. Anal.* **2021**, *124*, 105336. [CrossRef]
23. Luo, G.; Mo, Y.; Wu, C.; Zhang, F.; Liu, L.; Chen, W. Experimental study of ice impact on aluminium/carbon fiber reinforced composite dual plate. *Int. J. Crashworthiness* **2022**, *27*, 510–521. [CrossRef]
24. Luo, G.; Zhang, F.; Xu, Z.; Zhang, H.; Liu, L.; Chen, W. Internal reinforcement mechanisms for gelatin bird projectiles for artificial bird impact tests. *Mech. Adv. Mater. Struct.* **2023**, *30*, 3075–3085. [CrossRef]
25. Zhang, F.; Luo, G.; Zhang, H.; Cong, P.; Liu, L.; Chen, W. Experimental and numerical analysis study on the low and medium speed bird strike. *Eng. Fail. Anal.* **2024**, *156*, 107766. [CrossRef]
26. Zhou, R.; Liang, B.; Yue, Z.; Yang, H.; Zou, C.; Zhang, F.; Chen, S. High fidelity simulations of bird impact damages of a 5 MW wind turbine composite blade using SPH and damage models. *Thin-Walled Struct.* **2025**, *208*, 112835. [CrossRef]
27. Papadakis, M.; Yeong, H.; Suares, I.; Jacob, J. Experimental and computational investigation of ice shedding from aircraft surfaces. In Proceedings of the 44th AIAA Aerospace Sciences Meeting and Exhibit, Reno, NV, USA, 9–12 January 2006.
28. Papadakis, M.; Yeong, H.; Suares, I. Simulation of ice shedding from a business jet aircraft. In Proceedings of the 45th AIAA Aerospace Sciences Meeting and Exhibit, Reno, NV, USA, 8–11 January 2007.
29. Papadakis, M.; Yeong, H.; Shimoi, K.; Wong, S. Ice shedding experiments with simulated ice shapes. In Proceedings of the 1st AIAA Atmospheric and Space Environments Conference, San Antonio, TX, USA, 22–25 June 2009.
30. Mi, B.; Zhan, H. Numerical simulation on rigid foreign object exclusion in the turboprop engine intake system with a bypass duct. *IEEE Access* **2019**, *7*, 61920–61933. [CrossRef]

31. Wang, L.; Zhang, Y.; Mi, B.; Yang, M. Numerical simulation on excluding foreign objects from engine inlet of turboprop aircraft. *Adv. Aeronaut. Sci. Eng.* **2020**, *11*, 264–271.
32. Park, C.Y.; Jang, B.W.; Kim, J.H.; Kim, C.G.; Jun, S.M. Bird strike event monitoring in a composite UAV wing using high speed optical fiber sensing system. *Compos. Sci. Technol.* **2012**, *72*, 498–505. [CrossRef]
33. Chen, X.; Liu, J.; Jiang, C.; Zhao, Z.; Zhang, H.; Zhang, C.; Li, Y. Evaluation of a substitute bird for engine fan blade impact tests considering the bird-slicing state. *Eng. Fail. Anal.* **2025**, *167*, 109056. [CrossRef]
34. Lavoie, M.; Gakwaya, A.; Ensan, M.N.; Zimcik, D.; Nandlall, D. Bird's substitute tests results and evaluation of available numerical methods. *Int. J. Impact Eng.* **2009**, *36*, 10–11. [CrossRef]

Disclaimer/Publisher's Note: The statements, opinions and data contained in all publications are solely those of the individual author(s) and contributor(s) and not of MDPI and/or the editor(s). MDPI and/or the editor(s) disclaim responsibility for any injury to people or property resulting from any ideas, methods, instructions or products referred to in the content.